Structural lightweight concrete: recent research

Joost Walraven, Joop den Uijl, Jan Stroband, Nazeh Al-Zubi Delft University of Technology

Jan Gijsbers, Marius Naaktgeboren TNO Building & Construction, Rijswijk

As a result of a number of reasons new interest developed into the use of lightweight aggregate concrete. Within the scope of this development, a modernized code for lightweight concrete had to be written. In order to support this development, a number of research projects have been carried out. The aim of the research was to verify the appropriateness of a number of design methods for lightweight concrete. The behaviour of various types of lightweight concrete has been studied.

Keywords: Lightweight concrete, material properties, concentrated loading, splitting, bond, crack width, shear

Introduction

The development and application of concrete with artificially produced lightweight aggregates has also in the Netherlands a long history. After the rise of the production costs due to the energy crisis in the seventies, however, the material lost its competitiveness on the market. In the eighties, the increasing engagement in environmental problems leaded to a revival of the material. On the one hand the sand and gravel resources in the Netherlands became a matter of concern, on the other hand solutions were sought for the increasing quantities of fly ash, released as a rest-product in coal-furnished energy production plants. The use of this material for the fabrication of lightweight aggregate particles contributed, as such, to the solution of both problems.

After an evaluation of the first experiences with Lytag aggregate (CUR 1989), a new CUR Committee "Lightweight Concrete" was installed, with the aim to investigate in which respects the structural behaviour of lightweight concrete deviates from that of normal weight concrete and to what extent the behaviour of lightweight concrete is governed by specific material properties like tensile strength, aggregate interlock and fracture energy. The research program focused on structural mechanisms, which may logically be expected to be specially influenced by these properties, such as the shear -, bond - and splitting behaviour. The results of these investigations will be presented in the sequel.

Material properties

In this research program three types of lightweight aggregate have been used. These aggregates are indicated here with their trade-mark: Lytag, Aardelite and Liapor. Lytag is made from pulverized fly ash mixed with powder coal particles, which are sintered at a temperature of about 1100°C.

Aardelite consists of a mixture of fly ash, limestone and sand. The volume weight of Aardelite and Lytag are at the upper limit of what is usual for lightweight concrete (Table 1); therefore also a much lighter particle (Liapor, sintered slate) was involved into the investigation. The pursued cubestrengths after 28 days were 30 MPa and 60 MPa. To make a distinction between those strength-classes the symbols B30 and B60 are used. For the sake of comparison also normal weight concretes B30 and B60 have been tested.

Table 1. Volume weight and maximum moisture content.

Type of aggregate	Mass density ¹ (kg/m ³)	Moisture content ² (%)		
Lytag 4–8	1385	15		
Lytag 6-12,5	1430	13		
Aardelite 4–16	1630	18		
Liapor 4–16	940	21		

dry.

The most important mix properties are listed in Table 2. For the fine aggregate fraction river sand was applied. The volume-ratio between lightweight aggregates and sand amounted to 2:3. All types of lightweight aggregate were saturated with water before mixing (24 hours submerging, 3 hours leakage).

Table 2. Mixture properties.

Type of aggregate	Gravel	Gravel	Lytag	Lytag	Aardelite	Liapor
strength class	B3()	B60	B30	B60	B30	B30
cement content (kg/m³)	291	318	298	364	301	318
Portland cement type	A	В	А	В	A	Α
lightw.aggr./sand (V/V)	-	-	40/60	40/60	39/61	39/61
Lytag 4/6:Lytag 6/12.5	-	-	34/66	35/66	-	_
superplasticizer	-	2	-	1.5	-	-
(mass % Cem)						
water/cement ratio1	0.60	0.43	0.69	0.44	0.66	().44
slump (mm)	55	5	170	35	280	15
mass density mortar	2370	2367	1938	2003	2095	1728
(kg/m^3)						

without adsorbed water.

The properties of the concrete at 28 days are given in Table 3. These values apply particularly to that part of the project which focused on bond, see chapter 4.1. The ratio between the compressive strengths measured on prisms $(100 \times 100 \times 400 \text{ mm})$ and on cubes (150 mm) was about 0.75 for

Lytag, Aardelite and Gravel and 0,85 for Liapor. The ratio between splitting tensile strength and cube compressive strength was in good agreement with the relation

$$f_{\text{ct,sp}} = 0.24 f_{\text{cc}}^{2.3} \text{ with } f_{\text{ct}} \text{ and } f_{\text{cc}} \text{ in MPa}$$
 (1)

both for normal – and for lightweight concrete. The splitting tensile strength was measured on cubes which had hardened at 95% RV and 20°C. If the specimens had hardened in the testing hall, with about 65% RV and 18°C, the splitting tensile strength was about 10% lower, which was believed to be due to the influence of self equilibrating stresses due to drying. In Table 3 also the axial tensile strength is given. On average those values were about 10% lower than the values of the splitting tensile strength, which is a value which agrees with the corresponding relations given in Eurocode 2.

Table 3. Some mechanical properties of the investigated concrete types.

Concrete type	$f_{cc}(MPa)$	$f_{\rm ct.sp}({ m MPa})$	$f_{\rm ct}({\rm MPa})$	$E_{\varsigma}(\mathrm{MPa})$	$G_i(J/m^2)$	$l_{ch}(mm)$
Gravel B301	23.1	2.04	1.97	29800	78	599
Gravel B60	61.8	3.56	2.86	35900	108	474
Lytag B30	27.5	2.27	1.96	20400	63	335
Lytag B60	61.9	3.85	3.49	26900	76	168
Aardelite B30	24.1	2.11	2.03	21200	48	247
Liapor B30	27.5	2.61	2.00	18700	56	262

after 13 days, all others after 28 days.

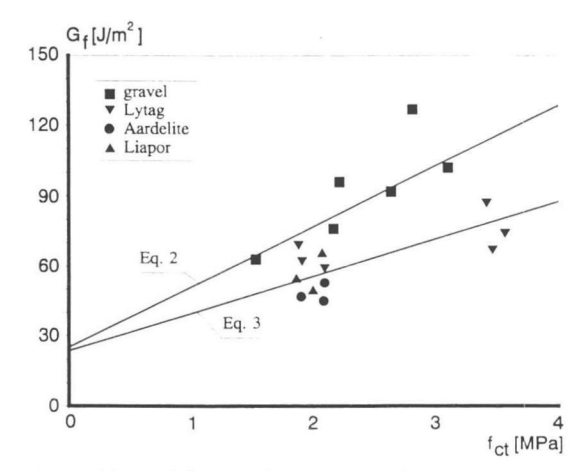


Fig. 1. Measured G,-values in comparison with Eq. 2 and 3.

² after 24 hours of submerging.

The values of the fracture energy G_t are represented in Fig. 1. For normal weight concrete Hordijk (1989) derived on the basis of a large number of test results the relation

$$G_t = 24 + 26 f_{ct} (J/m^2) \text{ with } f_{ct} \text{ in MPa}$$
 (2)

Fig. 1 shows, that the values obtained on the gravel aggregate concrete agree well with this expression. For lightweight concrete the best agreement is obtained with

$$G_{\rm r} = 24 + 16 f_{\rm ct} (J/m^2) \text{ with } f_{\rm ct} \text{ in MPa}$$
 (3)

Fig. 2 shows the averaged softening curves for the various concrete types. The softening curves for the lightweight concretes are steeper than for the gravel aggregate concretes, which can be explained on the basis of the smaller strength of the lightweight aggregates and the corresponding reduced crack arresting capacity.

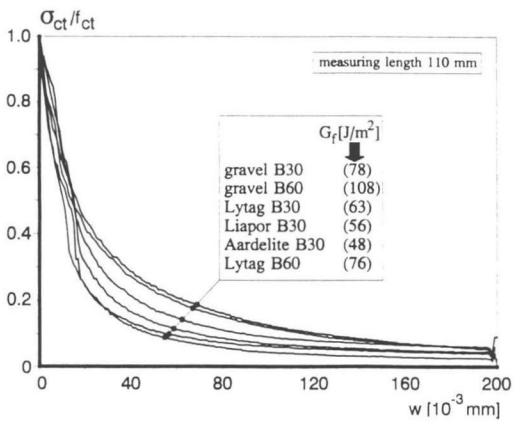


Fig. 2. Softening behaviour of the various concretes in tension.

For the shape of the softening curve Cornelissen et al., 1986, derived the relation

$$\frac{\sigma_{\text{ct}}}{f_{\text{ct}}} = \left(1 + \left(c_1 \frac{w}{w_o}\right)^3\right) e^{-c_2 - w - w} - \frac{w}{w_o} \left(1 + c_1^3\right) e^{-c_2}$$
(4)

with

w = crack width

 w_0 = reference crack width = 5.14 G_t/f_{ct}

 $c_1 = 3$

 $c_2 = 6.93$

This expression turned out to describe the experimental softening curves quite well. The best parameter to characterize the brittleness of a material, however, is the "characteristic length". This value, which is not a real length but a fracture mechanics parameter, is according to Hillerborg et al. (1976), equal to

$$I_{\rm ch} = E_{\rm c}G_{\rm r}/f_{\rm ct}^2 \tag{5}$$

A decrease of this value means a decrease of the toughness of the material. The last column in Table 3 shows, that lightweight concrete is more brittle than gravel aggregate concrete. The most brittle behaviour is found for Lytag B60.

Introduction of concentrated loads

Because lightweight concrete has a tendency to behave in a more brittle way than normal weight concrete, special attention should be given to load bearing mechanisms, where spalling or splitting actions govern the behaviour. This can for instance be expected if large forces act on a small area, such as at bearings or at the introduction area of prestressing forces.

To study this phenomenon, two types of tests on plain concrete specimens have been carried out. In one series of tests, Fig. 3a, the ratio between the width of the loading area and the width of the specimen was varied. In the second series the loading area was always quadratic. The centre of this area was eccentric with regard to the specimen axis and the area was varied in size, see Fig. 3b. The aim of these tests was to study the influence of the type of aggregate, the strength, and the dimensions of the loaded area with regard to the specimen dimensions. This was felt to be specially of interest, because of the fact that mechanisms, governed by the tensile strength of the concrete are often considerably size-dependent, Walraven (1993).

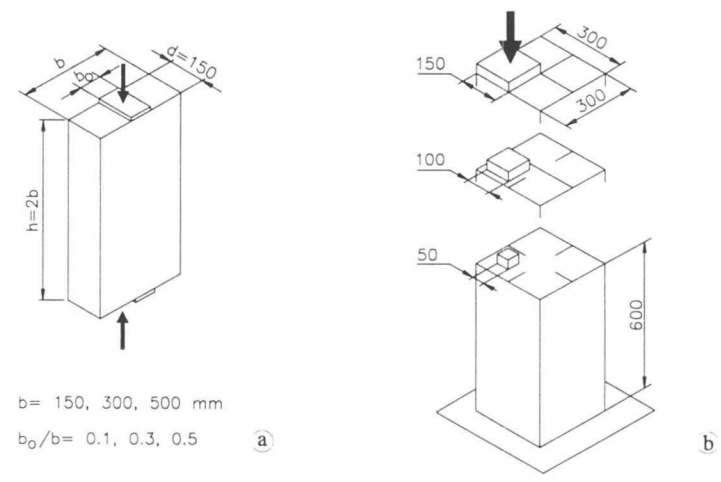


Fig. 3a. Splitting line loads on prismatic specimens.

3b. Concentrated loads on prismatic specimens.

Splitting test on prismatic specimens

In this part of the tests, Fig. 3a, the most important parameter was the ratio between the width of the loading area and the width of the specimen, which varied between 0.1 and 0.5. Between the loading plate and the specimen, an intermediate layer of cardboard was applied.

Fig. 4 shows the effect of the width of the loading plate on the maximum stress reached under this plate, for constant specimen dimensions 300×600 mm. In the investigated range, with

 $b_o/b = 0.1$, 0.3 and 0.5, no significant influence of the concrete type on the ultimate bearing capacity was observed.

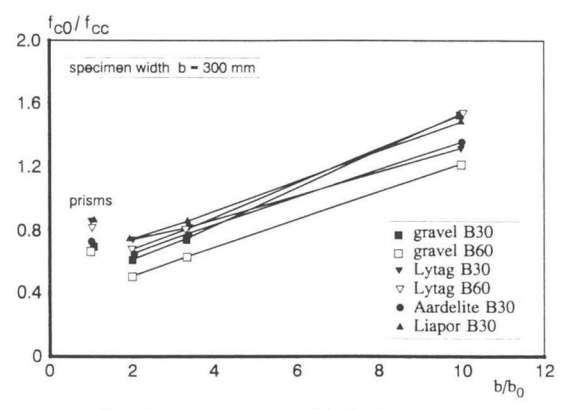
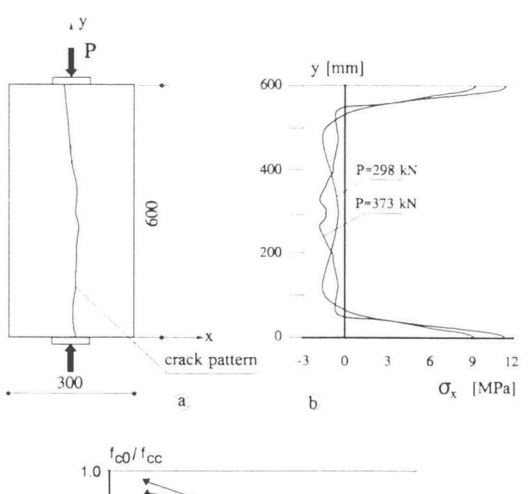


Fig. 4. Effect of the relative width of the loading plate on the maximum stress f_m reached at the loaded area.



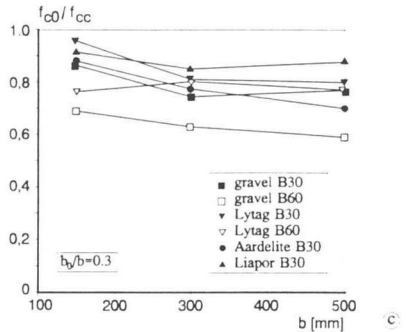


Fig. 5. Splitting tests on specimens with various sizes.

Fig. 5 shows the results of a series of tests in which the ratio between the width of the loading plate and the specimen width was kept constant at 0.3. The specimens had a thickness of 150 mm and a width to depth ratio of 1:2. A basic series consisted of 3 specimens with depths of 300, 600 and 1000 mm. Fig. 5a shows a cracked specimen with h = 600 mm.

Fig. 5b shows the stresses along the longitudinal axis of the specimen, calculated with the nonlinear FEM-program DIANA. Just below the loading plate, in the transverse direction, compressive stresses occurred under a steep gradient. In the inner part, over about 80% of the specimen length, the tensile stresses remained approximately constant. This shows that the redistribution capacity after the occurrence of a splitting crack is limited. In nearly all the cases after the occurrence of a longitudinal crack no further increase of the load was possible. Therefore the size dependency is weak, as follows from Fig. 5c.

The behaviour of the specimens during testing could be adequately described with the nonlinear FEM-analysis. Therefore, subsequently to the tests, some parameter studies have been carried out in order to find the influence of the most important variables f_{ct} (tensile strength) and G_t (fracture energy). Fig. 6. shows the calculated maximum loads as a function of f_{ct} and G_t .

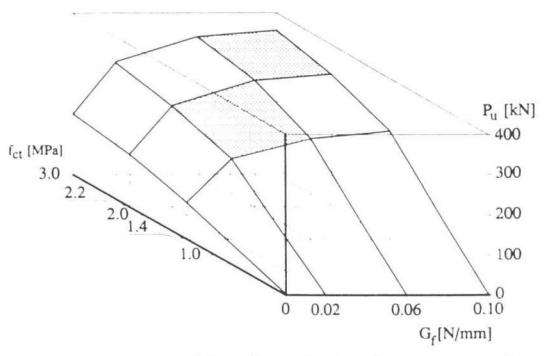


Fig. 6. Dependence of the splitting load on the concrete tensile strength f, and the fracture energy G.

Behaviour of the specimens under eccentric concentrated loads

Although the fracture mechanics parameters of the lightweight concretes significantly differ from those of normal weight concrete, in the previously described tests series no evident differences have been observed between the lightweight and the normal weight concrete specimens. In order to verify, whether this is also the case if the load spreads into two directions, the behaviour of prisms under eccentric concentrated loading was investigated (Fig. 3b). This part of the experimental program consisted of five series of three specimens each, with which the influence of the following parameters was investigated:

- dimensions of the loaded area
- type of aggregate
- strength of the concrete

In the specimens with the larger loading plates, failure occurred due to shearing off of a corner of the specimen. In the case of the smaller loading plates a cone was formed under the loading plate which was followed by splitting of the specimen, Fig. 7.

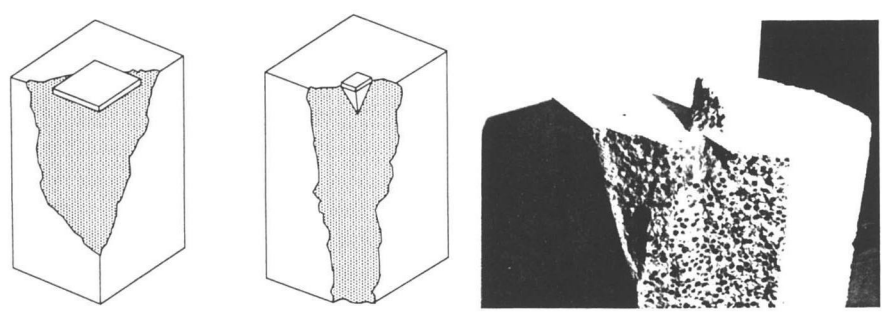


Fig. 7. Failure modes for eccentric concentrated loading.

Fig. 8 shows the influence of the loading plate dimensions on the maximum stress under these plates. For normal weight concrete this maximum stress was proportional to $(A/A_o)^{0.5}$ and for Liapor with $(A/A_o)^{0.33}$, where A_o denotes the loaded area and A is the maximum area corresponding geometrically to A_{ox} having the same centre of gravity, which is possible to inscribe in the cross-section considered, see also Fig. 8. This agrees with observations made by Heilmann (1983). The other lightweight-concrete types gave values between those limits. It turned out that the ultimate stress at the loaded area depends on the oven-dry density of the concrete in kg/m³ and the ratio A/A_{ox} which can be formulated as:

$$f_{co} = f_{cc} (A/A_o)^{\rho/4800} \tag{6}$$

This is shown in Fig. 9.

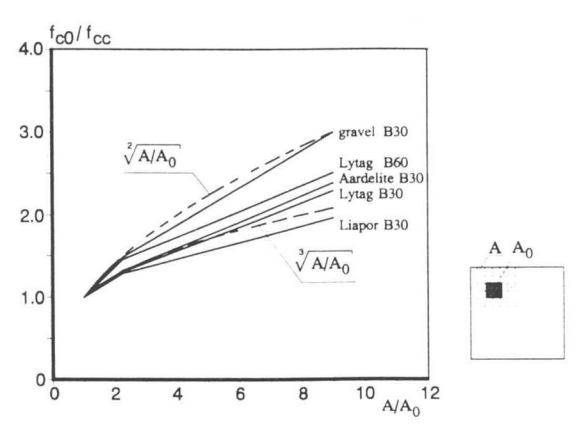


Fig. 8. Influence of the size of the loading plate on the ultimate stress under this plate.

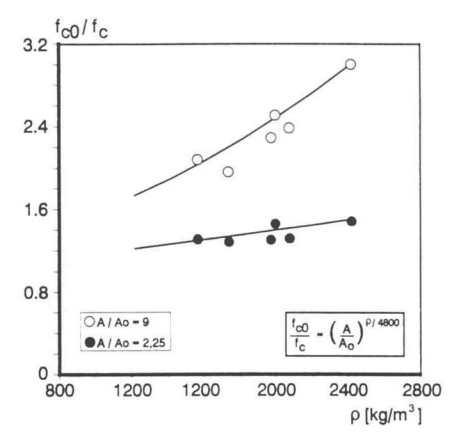


Fig. 9. Influence of the dry-density of the concrete on the maximum stress reached under the loading plate.

Bond and tension-stiffening

Pull-out tests

Pull-out tests have been carried out on cube-shaped specimens with centric bars, which were bonded over a length of three times the bar diameter, Fig. 10. The pull-in displacement of the bars with regard to the concrete was measured at the non-tensioned side by an LVTD. The displacement at the tensioned side has been calculated from this value, by assuming that the bond stress is constant over the bonded length. The corresponding steel stress distribution is linear.

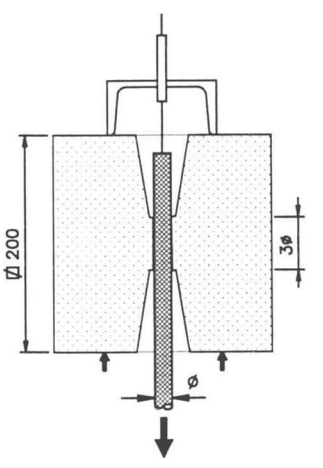


Fig. 10. Experimental set-up of pull-out test.

The results of the tests on the various concrete types are represented in Fig. 10. It turned out that the bar diameter had no significant influence on the results. Fig. 11a shows that the bond strength of the lightweight concrete is always lower than that of the normal weight concrete, both for B30 and for B60.

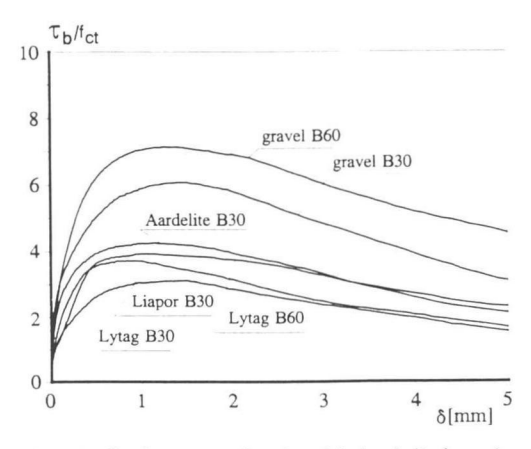


Fig. 11. Bond stress as a function of the bond-slip for various concrete types.

Since the bond strength is always assumed to be narrowly related to the tensile strength of the concrete, in Fig. 11 the ratio bond-stress to tensile strength has been represented as a function of the bond-slip. This diagram shows, that the relative bond strength of the lightweight concretes is always lower than that of the corresponding normal weight concretes. The various lightweight concretes show a similar behaviour, in spite of their differences in mass density. Obviously the bond resistance of lightweight concrete is significantly governed by the reduced strength of the lightweight aggregate particles.

Tension-stiffening tests

Tension-stiffening tests have been carried out on specimens like shown in Fig. 12. Fig. 13 shows some representative results for specimens reinforced with a centric bar *o* 12 mm. The influence of the concrete type on the behaviour is narrowly related to the concrete tensile strength. It is shown that, with regard to the effect of tension stiffening, hardly differences exist between lightweight and normal weight concrete specimens, in spite of the differences between the bond stress – bond slip curves (Fig. 11). This contradiction is only apparent, because the slip in the tension stiffening tests mostly did not exceed a value of 0.2 mm, whereas the maximum values in the direct bond tests have been reached at a slip of about 1 mm. The differences in bond between the various concretes at a slip smaller than 0.2 mm are relatively small (Fig. 11).

The CEB/FIP Model Code for Concrete Structures 1990/1993 gives relations for the effect of tension-stiffening and crack width, which are based on the "rigid-plastic" bond-slip relation, shown in Fig. 14a. The steel stress versus total strain relation of the reinforced concrete bar, calculated on the basis of Fig. 14a, is shown in Fig. 14b. In this diagram, stage 1 is the "crack formation stage".

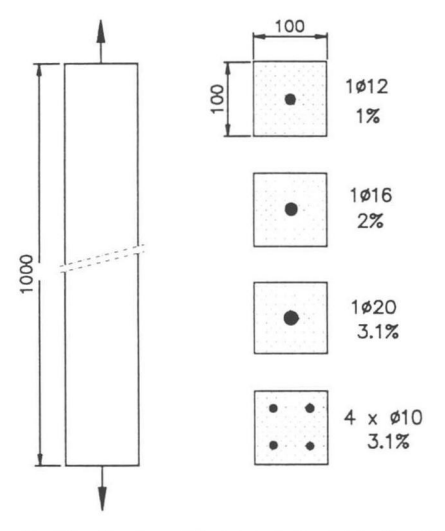


Fig. 12. Tension-stiffening tests on centrically reinforced concrete bars.

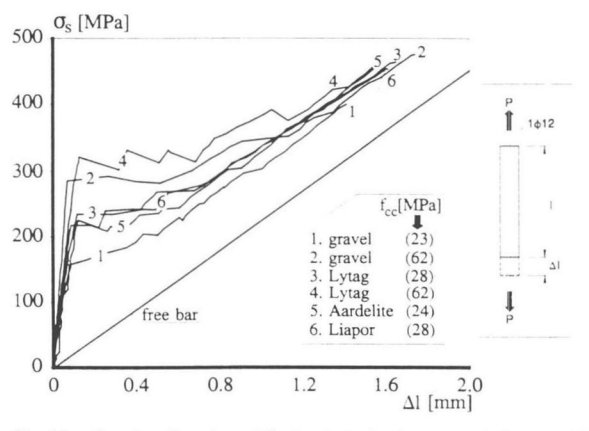


Fig. 13. Results of tension-stiffening tests for the same reinforcement but different concretes.

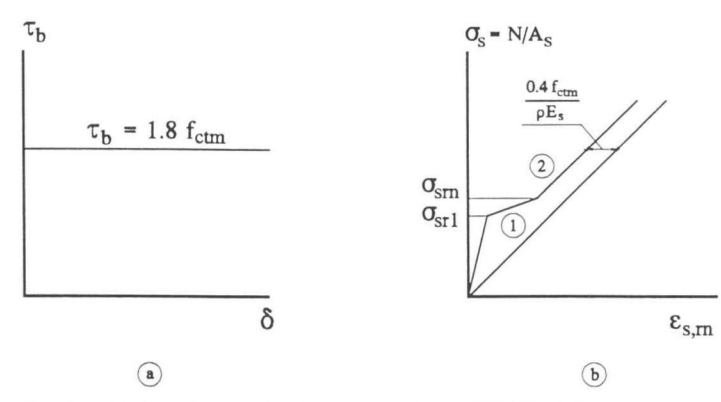


Fig. 14a. Basic bond stress-slip diagram, according to CEB, 1990/1993.

14b. Resulting steel stress-total strain relation.

If the tensile strength of the concrete is considered to be constant, this results in a horizontal "plateau". In reality, cracking occurs gradually in sections with larger tensile strengths, so that the line 1 will have a small inclination ($\sigma_{sm} > \sigma_{sr1}$) with generally $\sigma_{sm} \approx 1.15 \ \sigma_{sr1}$). Stage 2 is the stabilized cracking stage, in which no new cracks occur, but in which the existing cracks become wider as a function of the increasing tensile force N. These formulations are simple and efficient. Fig. 15 shows, for Lytag B30, some tension-stiffening relations observed in the experiments in comparison with the calculated ones: the figures refer to the tests with a single bar ϕ 12 and ϕ 16 respectively. The agreement is seen to be good.

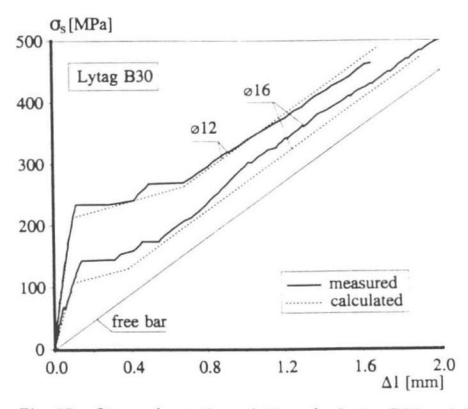


Fig. 15. Stress-elongation relations for Lytag B30, reinforced with one bar φ12 or one bar φ16.

Further to this, Fig. 16 shows the average crack widths observed in all the tests at a steel stress of 300 MPa. The diagram confirms the, well-known, favourable influence of smaller diameters. Specially for the smaller diameters, the influence of the concrete strength is evident. On the

contrary, the influence of the concrete type is limited. In a general sense, it can be concluded, that there are no significant differences between normal weight concrete and lightweight concrete as far as the cracking behaviour is concerned.

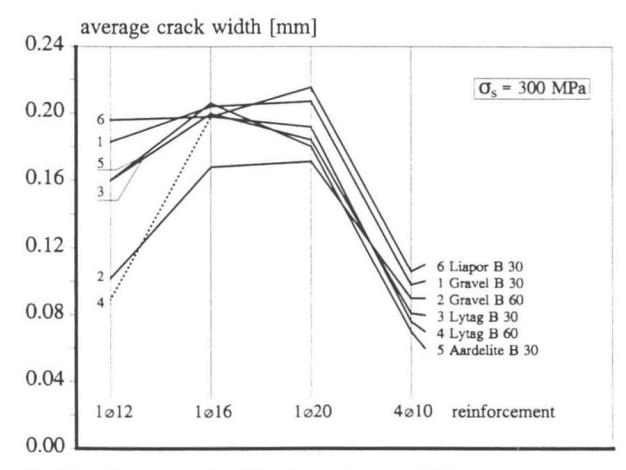


Fig. 16. Average crack widths at a steel stress of 300 MPa.

Also with regard to the calculation of the crack widths, the CEB/FIP Model Code 90/93 gives simple expressions, which have been derived on the basis of the relation shown in Fig. 14a. As an example, the average crack widths are calculated for the Lytag B30 specimens, reinforced with 1 ϕ 12, 1 ϕ 16, 1 ϕ 20 and 4 ϕ 10 respectively, at a steel stress $\sigma_s = 300 \text{ N/mm}^2$.

According to the CEB/FIP Model Code, Chapter 7.4.3, the following conditions and relations apply:

- stabilized cracking stage
- average crack distance is:

$$\bar{s} = \frac{2}{3} \frac{\phi}{3.6\rho} = 0.185 \phi/\rho \tag{7}$$

- for a bar with a length *l* the number of cracks is

$$n = l/s - 1 \tag{8}$$

- the average strain of the total bar is

$$\varepsilon_{\rm m} = \varepsilon_{\rm s} - \frac{0.6 f_{\rm ctm}}{E_{\rm s} \rho} = \frac{\sigma_{\rm s}}{E_{\rm s}} - \frac{0.6 f_{\rm ctm}}{E_{\rm s} \rho} \tag{9}$$

where σ_{i} is the steel stress in a crack.

- the average crack width is

$$w_{\rm m} = \varepsilon_{\rm m} \cdot \tilde{s}$$
 (10)

For Lytag B30 the average axial tensile strength was $f_{\rm vim}$ = 2.0 MPa (Table 3). This results in the values, listed in Table 4. The agreement between experimental and calculated values is seen to be good.

Table 4. Number of cracks and average crack-widths for Lytag B30: experiments versus calculations.

		number of cracks		av. crack width		
	\tilde{s}_{cale} (mm)	$n_{\rm calc}$	H_{exp}	$w_{\rm calc}({ m mm})$	$w_{\rm exp}({ m mm})$	
<i>p</i> 12	196	4	5	0.18	0.16	
1 6	147	6	5	0.18	0.20	
2 0	118	7	6	0.15	0.18	
4 φ 1()	59	16	14	0.08	0.08	

Lapped splices

In the pull-out tests, described earlier, the cover was large enough to prevent splitting failure. In the case of smaller covers, however, splitting will govern the failure behaviour, so that the required anchorage length and overlapping length should depend on the concrete cover. In order to find out if in this respect differences between lightweight and normal weight concretes exist, a number of four-point bending tests have been carried out on beams with lapped splices. The ribbed bars FeB 500 had a diameter of 20 mm. The concrete cover was 30 or 60 mm (corresponding to 1.5ϕ and 3ϕ respectively), and the centre to centre distance of the bars was 80 mm (corresponding to 4ϕ). In the beams made of Liapor concrete the overlapping length was varied between 20ϕ and 50ϕ : in the other beams this length was 30ϕ . In one beam 50% of the bars was lapped, in the other beams 100%. In one beam closed stirrups were applied in the overlapping area. In the other cases the transverse reinforcement was anchored by means of anchor-plates in order to simulate the conditions in a wide slab (Fig. 17).

Both the development of the cracking pattern and the failure behaviour of all the beams with 100% lapped bars showed a large similarity. At the end of the lapped splices the crack width was about twice as large as observed in the regions outside the splices. At the onset of failure, splitting cracks occurred at the sides of the beams in the splice- area and a sudden failure was observed in combination with total spalling-off of the concrete cover over the splice-area. The last phenomenon was avoided by the use of closed stirrups, but in this case the capacity decreased very rapidly after reaching the maximum load (Fig. 18). The beams in which only 60% of the bars were lapped showed a much more ductile behaviour.

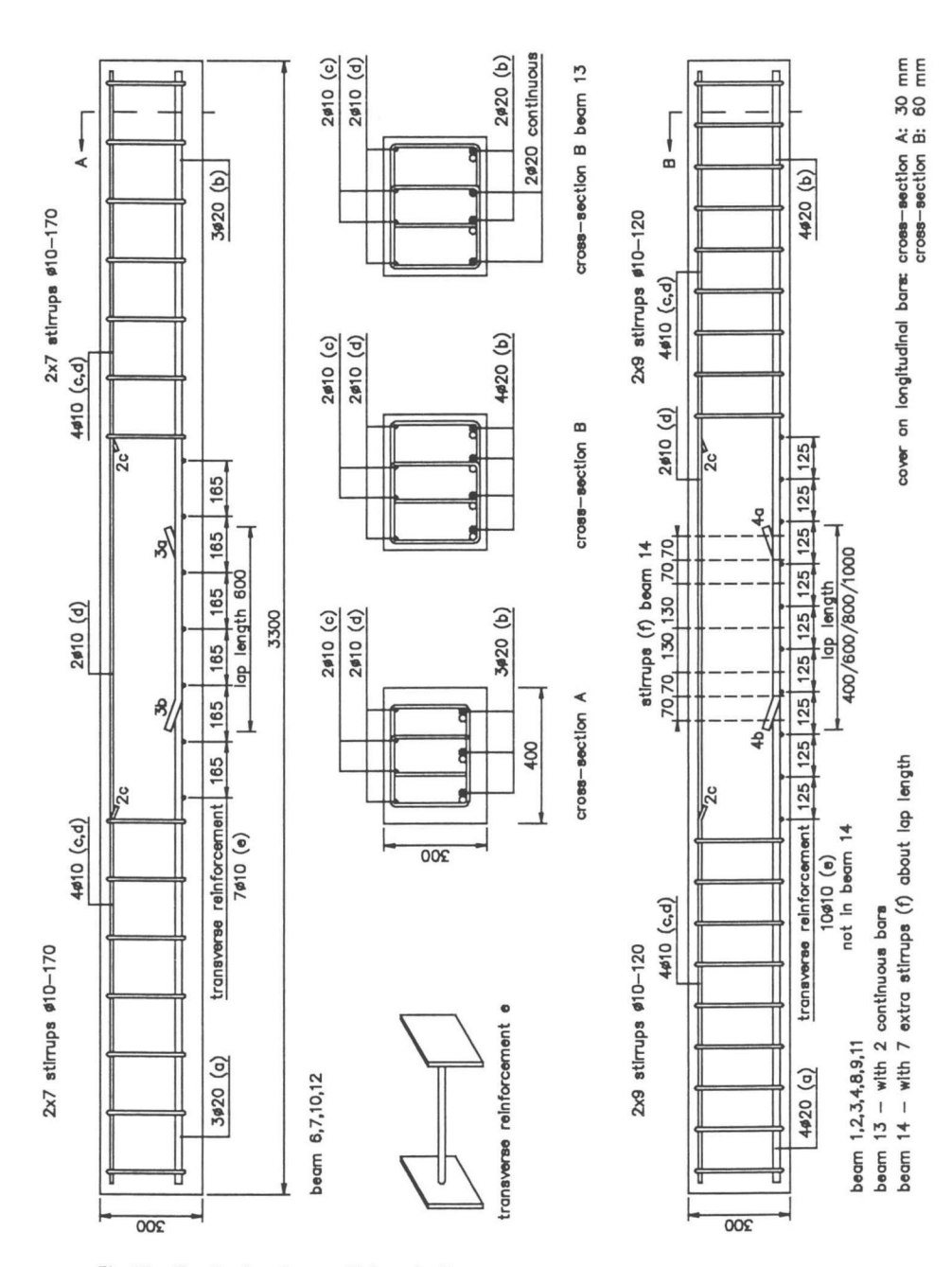


Fig. 17. Details of specimens with lapped splices.

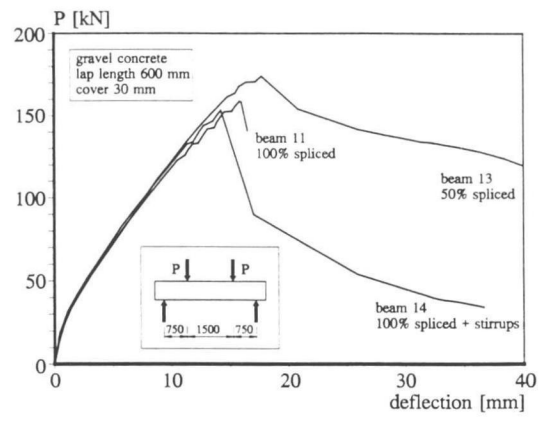


Fig. 18. Influence of the percentage of lapped bars and the application of stirrups on the load-deflection relation.

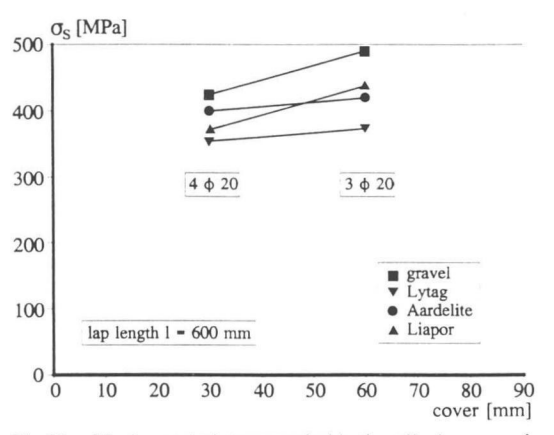


Fig. 19. Maximum steel stress reached in the spliced area as a function of the concrete type and the cover.

On average the maximum steel stress reached during loading was in lightweight concrete about 15% smaller than in normal weight concrete (Fig. 19). The required overlapping length, however, is more than 15% larger, because the maximum stress is less than proportional to this length (Fig. 20).

The results obtained in this part of the research program are in agreement with the results obtained by Betzle et al. (1983).

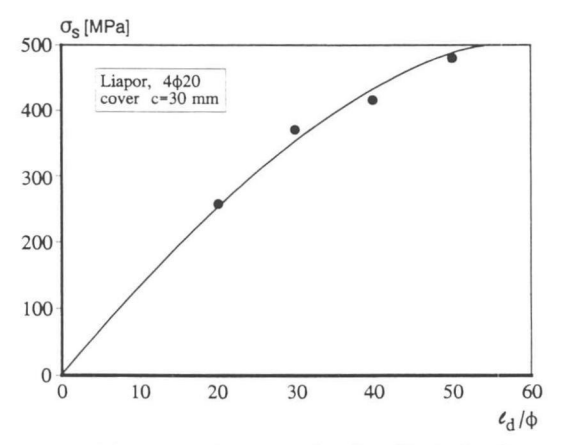


Fig. 20. Maximum steel stress as a function of the lap length.

Shear

Modern calculation methods for the shear carrying capacity of beams provided with shear reinforcement take into account the possibility of rotation of the compression struts. In the Eurocode 2, in chapter 4.3.2.4.4, for normal weight concrete the "variable strut inclination method" is presented. Using this method, the designer is allowed to choose the angle θ of the strut inclination between

$$0.4 < \cot \theta < 2.5 \tag{11}$$

which means that θ may be chosen between 22° and 68°. The choice of the lower value of 22° will normally lead to the most economic design. In this case the compression strut direction is supposed to rotate from an initial value of 45° to a lower value of 22°. It is believed that the capacity of cracks to transmit shear forces, by aggregate interlock, is an important precondition for sufficient redistribution capacity. In gravel aggregate concrete the cracks are rough, because the strong and hard aggregate particles extend from the crack faces and work as shear displacement arresters, Walraven 1980. However, in lightweight concrete the cracks intersect the aggregate particles, so that the crack faces must be much smoother. It is therefore questionable, whether in lightweight concrete the redistribution capacity is equally good as in gravel concrete. This question was the main object of investigation in this part of the research program.

Altogether five series of three beams have been tested. The cross-section of a beam and a longitudinal view with an indication of the positions of the measuring devices are shown in the Figures 21 and 22. Fig. 22 shows at the lefthand side of the beam a grid with metallic points, stuck on the concrete surface, with which the displacements of the crack faces have been measured. At the

righthand side a combination of LVTD's is applied, with which the general deformations of the web can be measured. On the basis of these deformations the principal strain directions can be calculated.

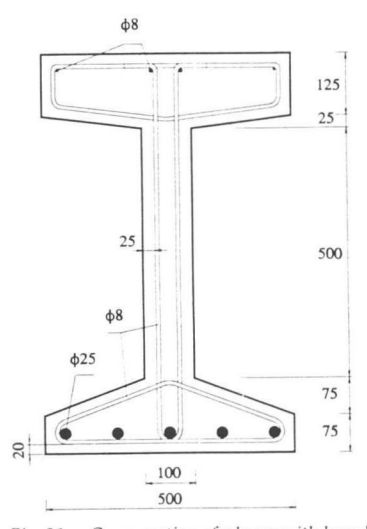


Fig. 21. Cross-section of a beam with low shear reinforcement ratio.

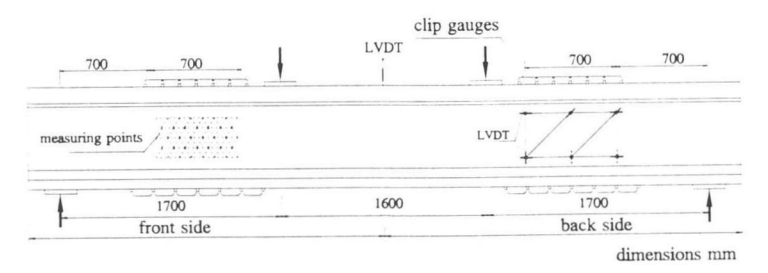


Fig. 22. Lateral view of a beam with measuring devices.

Within one series, the concrete type was kept constant and only the shear reinforcement was varied. The values of the shear reinforcement ratio within one series were 0.43%, 0.89% and 1.45% respectively. In the beams with the lowest shear reinforcement ratio's shear failure was always preceded by yielding of the stirrups. In the beams with the highest shear reinforcement ratio web crushing always occurred before the stirrups yielded.

The behaviour which was observed can principally be described by a number of curves, Fig. 23:

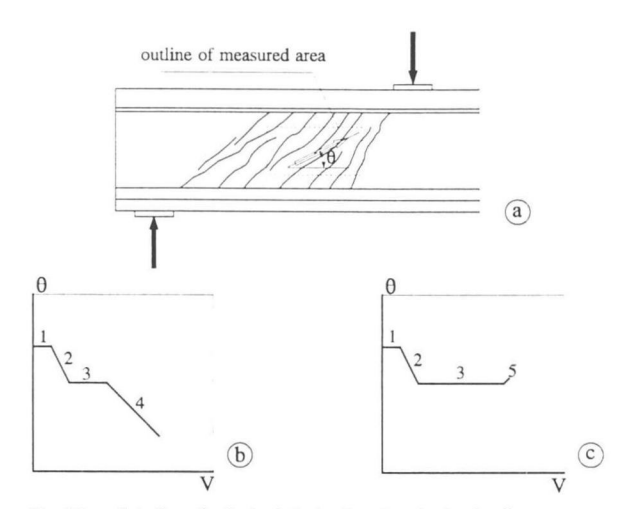


Fig. 23a. Rotation of principal strain direction during loading.

- 23b. Rotation in beams with low shear reinforcement ratio.
- 23c. Rotation in beams with high shear reinforcement ratio.
- before inclined cracking the principal strain direction is about 45° (curve 1);
- during inclined cracking the stiffness properties of the web are changed and the principal strain direction rotates to a lower angle (curve 2);
- when the cracking pattern has stabilized, the inclination remains constant. In this stage both concrete and steel are in the elastic state (curve 3);
- when the stirrups start to yield, the shear capacity can only be enlarged by a further rotation of the struts (curve 4, Fig. 23b), so that more stirrups are mobilized for the transmission of the shear force. The consequence of the lower inclination is, however, an increase of the inclined compressive stresses in the web concrete. When the ultimate strength of the concrete is reached failure occurs due to web crushing;
- if the shear reinforcement ratio is very high, the yielding stress of the steel is not reached.
 The concrete reaches its softening branch and even tries to maintain equilibrium by rotating back to a larger angle (line 5, Fig. 23c). Due to the relative brittleness of the concrete this backward rotation is limited.

Fig. 24 shows the measured behaviour for the series of three gravel aggregate beams B30 (Fig. 24, left), in comparison with the Aardelite-lightweight beams (Fig. 24, right).

The letters at the end of the identifying codes stand for \underline{L} ow, \underline{M} edium and \underline{H} igh shear reinforcement ratio's. The figures show, remarkably, that there is hardly any difference in behaviour between the gravel aggregate concrete and the lightweight concrete of the same strength. This holds true for all other lightweight concretes as well.

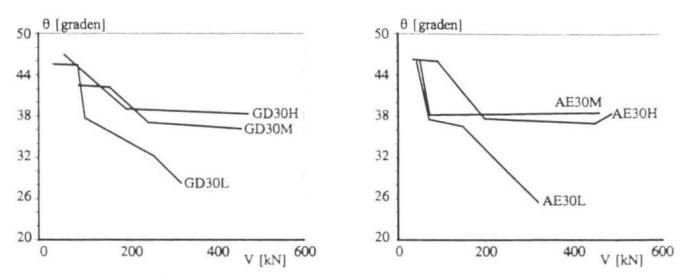


Fig. 24. Principal strain directions as a function of the shear force for gravel concrete (left) and Aardelite (lightweight) concrete (right), for high (H), middle (M) and low (L) shear reinforcement ratio.

The explanation for the fact that the strut-rotation in the lightweight concrete beams is about the same as in the normal aggregate concrete beams, is that in lightweight concrete the cracks, in spite of the broken aggregates, have a sufficient ability to transmit shear forces as a result of the irregular general shape of the crack faces, by virtue of which alternative contact areas develop during shear displacements. Fig. 25 shows an inclined crack in a lightweight concrete beam, in which it can be clearly seen, that local crushing of the concrete occurs due to the transmission of large concentrated forces across the crack.

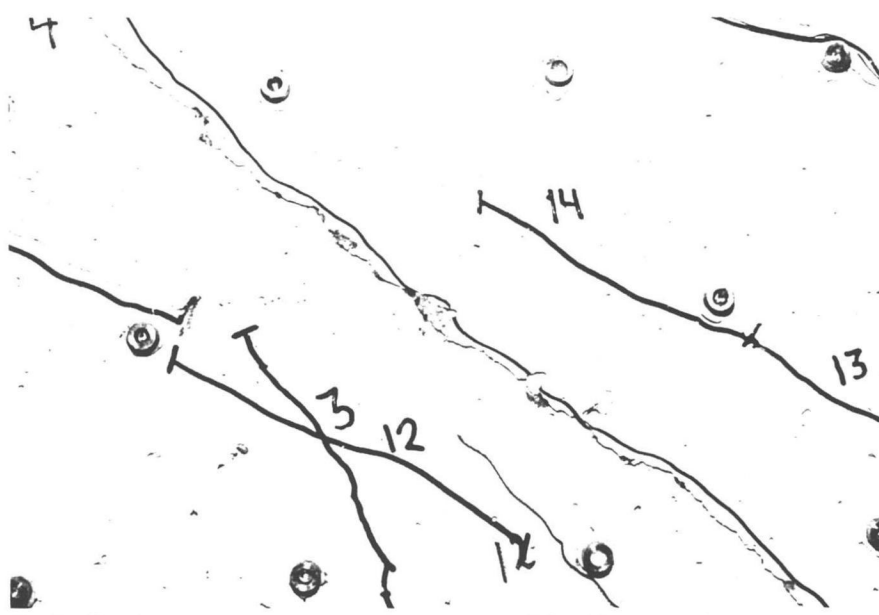


Fig. 25. Crushing at local contact areas in an inclined crack in lightweight concrete due to the transmission of forces across the crack.

It was measured that the shear displacements of the crack faces in lightweight concrete were twice as large as in normal weight concrete, at the same external load.

The results will be evaluated using the variable strut inclination method. This method is based on the lower bound solution of the theory of plasticity, Nielsen (1978). In order to explain this principle, two formulations for the shear capacity are used:

– If the concrete in the compression struts inclined to an angle θ reaches its crushing capacity, the corresponding shear force is

$$V_{u,2} = b_w z v f_c / (\cot \theta + \tan \theta)$$
 (12)

– If the (vertical) stirrups yield at a strut inclination θ , the corresponding shear force is

$$V_{u,3} = \frac{A_{sw}}{s} z f_{yw} \cot \theta \tag{13}$$

In those equations

 $b_w = \text{web width}$

 $z = inner lever arm \approx 0.9d$

s = stirrup distance

 f_{yw} = yield stress of stirrups

 θ = inclination of compression struts

 A_{sw} = cross-sectional area of one stirrup

v = effectiveness factor, taking account of the fact that the beam web is not as well suited to resist the inclined compression as test cylinders used to determine f.

 f_c = concrete cylinder strength

The theory of plasticity gives, as the best lower bound solution, the largest load satisfying the equations 12 and 13. Physically this means, that the strut inclination will decrease during loading, gradually mobilizing more yielding stirrups for resisting the applied shear, until in the inclined struts the concrete crushing strength $f_{cl} = yf_c$ is reached, Fig. 26.

Equalizing the equations 12 and 13 gives

$$\frac{v_u}{f_{c1}} = \sqrt{\psi(1-\psi)} \tag{14}$$

and

$$tan\theta = \sqrt{\frac{\psi}{1 - \psi}}$$
(15)

where

$$v_{\rm u} = V_{\rm u}/(b_{\rm w} \cdot 0.9d)$$

$$\psi = \frac{\rho_{siv} f_{uiv}}{f_{v1}}$$

with

$$f_{c1} = v f_{c}$$

Eq. 14 represents a circle in a v_u/f_{cl} ψ -coordinate system, see Fig. 27. The maximum value of v_u/f_{cl} is 0.5, which is obtained for ψ = 0.5.

It is found that when ψ runs from 0 to 0.5, ψ is running from 0 to 45°

For $\psi > 0.5$, the ψ -value is constant at 45°.

The complete solution for the load carrying capacity is thus

$$\frac{v_{\rm u}}{f_{\rm cl}} = \begin{cases} \sqrt{\psi (1 - \psi)} & \psi \le 0.5\\ 0.5 & \psi > 0.5 \end{cases}$$
 (16)

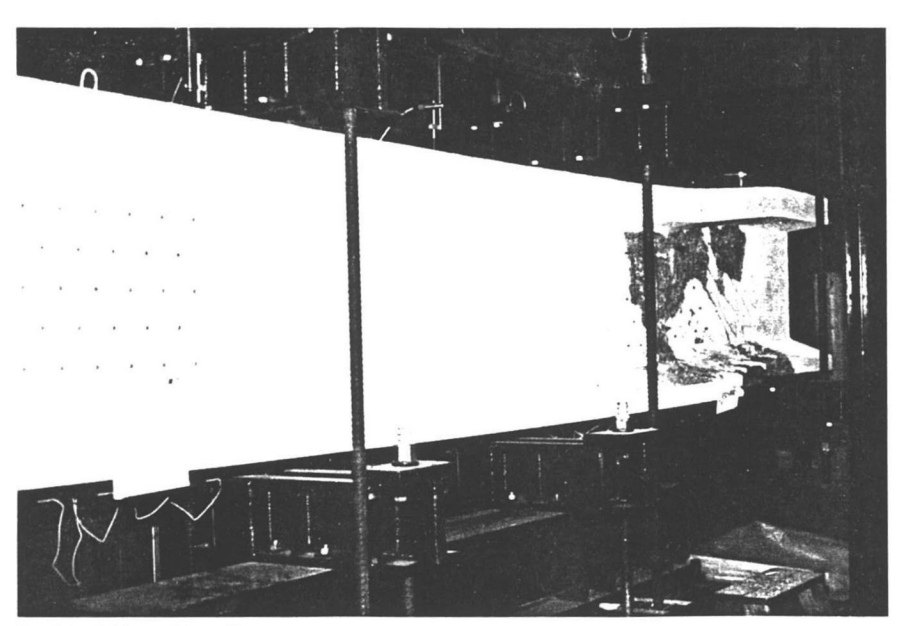


Fig. 26. Web crushing of beams.

with

$$f_{c1} = v f_{c}$$

See also Fig. 27.

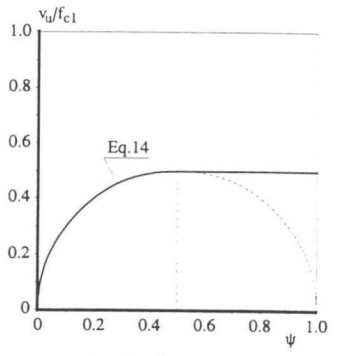


Fig. 27. Graphical representation of Eq. 14.

The equations (15) and (16) have been used as a basis for evaluation of the test results.

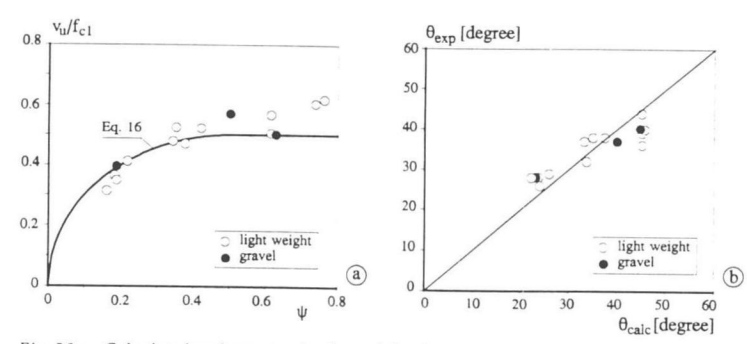


Fig. 28a. Calculated and measured values of the shear resistance.

28b. Calculated and measured values of the strut inclination.

Fig. 28a shows the test results in relation to Eq. 16.

A comparison between the calculated strut angles $\theta_{\rm calc}$ (Eq. 15) with the measured principal strain inclinations in the tests is given in Fig. 28b.

The best results were obtained with the well-known expression

$$v = 0.7 - \frac{f_c}{200} > 0.5$$

both for gravel aggregate and lightweight aggregate concrete.

The most important data of the tests are collected in Table 5.

Table 5. Results of shear tests on beams.

Beam		$f_c^{(2)}(MPa)$	$\rho_{sw}f_{sw}$ (MPa)	$\theta_{\rm meas}({ m degr})$	$V_{u,exp}(kN)$	$V_{\rm u.calc}({\rm kN})$	$\frac{V_{\text{u. exp}}}{V_{\text{u. calc}}}$
Ae1) 30	1	22.8	2.5	26	321	355	0.90
	m	21.7	5.4	38	457	431	1.06
	h	20.2	8.9	39	482	397	1.21
Gd 30	1	22.7	2.5	28	360	354	1.02
	m	17.6	5.4	37	420	368	1.14
	h	24.7	8.9	40	470	466	1.01
Lg 30	1	19.1	2.5	29	324	325	1.00
	m	28.4	5.4	37	520	512	1.02
	h	25.2	8.9	40	481	475	1.01
Lr 30	1	27.4	2.5	28	330	388	0.85
	m	25.0	5.4	38	461	475	0.97
	h	23.2	8.9	36	541	475	1.14
Lg 60	I	43.4	3.8	28	517	551	0.94
	m	46.3	7.6	32	751	680	1.10
	h	45.7	16.5	44	881	706	1.25

¹⁾ Ae = Aardelite Gd = Gravel ²⁾ Calculated from cube strength

 $\bar{x} = 1.04$ s = 0.11

Lg = Lytag with $f_c = 0.8 f_{cc}$

It can be concluded that, at least for the lightweight concretes tested, the redistributing capacity of the webs in shear is as good as in normal weight concrete. The measured strut rotations are the same and even the same effectivity factor for concrete crushing can be used.

Conclusions

- The splitting resistance of lightweight concrete in the case of the introduction of concentrated line loads does not significantly differ from that of normal concrete. The corresponding bearing capacity is hardly size-dependent.
- 2. If specimens are subjected to eccentrically applied concentrated loads, the bearing capacity is related to the concrete density through a power function.
- There is a significant difference between the basic bond-slip relations between normal weight and lightweight concrete. Nevertheless the description of the tension stiffening effect and the calculation of the crack widths can be carried out with the same expressions as used for normal weight concrete.

4. The shear behaviour of both the normal weight and the lightweight concrete beams tested can be well described with the variable strut inclination method. The observed behaviour was basically the same.

Acknowledgement

This publication has been issued in close cooperation with the Centre for Civil Engineering Research, Codes and Specifications.

Notations

b width

b_o width of loaded area

 $b_{\rm w}$ web width of beam

f_c cylinder compressive strength of concrete

 f_{cc} cube compressive strength of concrete

 $f_{\rm ct}$ axial tensile strength of concrete

 $f_{\rm ctm}$ average axial tensile strength of concrete

 $f_{\text{ct,sp}}$ concrete splitting strength

 f_{co} ultimate stress at loaded area

 $f_{\rm cl}$ compressive strength of concrete in inclined struts

f_{vw} yield stress of shear reinforcement

l_{ch} characteristic length

number of cracks

š average crack distance

s stirrup distance

w_m average crack width

z inner lever arm

A area

An loaded area

A_{sw} cross-sectional area of one stirrup

E_e modulus of elasticity of concrete

 G_i fracture energy

 $V_{\rm u}$ ultimate shear force

V_{u,2} ultimate shear force at inclined compression failure

V_{u.3} ultimate shear force at stirrup yielding

 ε steel strain

 $\varepsilon_{\rm m}$ average strain of reinforced concrete bar

 θ strut inclination

effectivity coefficient

- reinforcement ratio of reinforced concrete bar
- ρ_{sw} shear reinforcement ratio
- σ, steel stress

13 h

- φ bar diameter
- ψ mechanical reinforcement ratio

References

Betzle, M.S., Stockl, H., Kupfer, H. (1983), "Übergreifungs-Halbstoß mit kurzem Längsversatz bei zugbeanspruchten Rippenstählen in Leichtbeton, Deutscher Ausschuß für Stahlbeton, Heft 347, Berlin.

AND THE TREATMENT OF THE DESCRIPTION OF THE PROPERTY OF THE PR

- CEB/FIP Model Code for Concrete Structures (1990), CEB Bulletin d'Information, No. 213/214, May 1993.
- CORNELISSEN, H.A.W. (1986), HORDIJK, D.A. and REINHARDT, H.W., Experiments and theory for the application of fracture mechanics to normal and lightweight concrete, in "Fracture toughness and fracture energy", Elseviers Publishers.
- Heilmann, H.G. (1983), Versuche zur Teilflächenbelastung von Leichtbeton für tragende Konstruktionen, Deutscher Ausschuß für Stahlbeton, Heft 344, Berlin.
- HILLERBORG, A., Moder, M. and Petersson, P.E. (1976). Analysis of Crack Formation and Crack Growth by Means of Fracture Mechanics and Finite Elements, *Cement & Concrete Research*, 6, pp. 773–782.
- HORDIJK, D.A.(1990), Deformation controlled uniaxial tensile tests on concrete, TU Delft, Stevin-report 25.5.90-7/VFA,1990.
- NIELSEN, M.P., BRAESTRUP, M.W., JENSEN, B.C. and BACH, F. (1978), Concrete Plasticity, published by the Danish Society for Structural Science and Engineering.
- WALRAVEN, J.C. (1993), Size effects: Their Nature and Their Recognition in Building Codes, In Proceedings, JCI International Workshop on Size Effect in Concrete Structures, Sendai, Japan, pp. 295–314.
- WALRAVEN, J.C. (1980), Aggregate interlock: a theoretical and experimental investigation, PhD-Thesis, Delft University of Technology.